

Supplemental Material

Longitudinal multiorgan transcriptomic atlas of salt-induced hypertension

Ratnakar Tiwari^{1,*}, Olha Kravtsova¹, Lashodya V. Dissanayake¹, Melissa Lowe¹, Biyang Xu¹, Vladislav Levchenko¹, Steven Didik¹, Ruslan Bohovyk¹, Daria V. Ilatovskaya², Oleg Palygin³, Alexander Staruschenko^{1,4,5,*}

¹Department of Molecular Pharmacology and Physiology, University of South Florida, Tampa, FL 33602

²Department of Physiology, Medical College of Georgia, Augusta University, Augusta, GA 30912

³Department of Medicine, Division of Nephrology, Medical University of South Carolina, Charleston, SC 29425

⁴Hypertension and Kidney Research Center, University of South Florida, Tampa, FL 33602

⁵James A. Haley Veterans' Hospital, Tampa, FL 33612

Running title: Transcriptomic Atlas of Salt-Induced Hypertension

*Corresponding authors

Ratnakar Tiwari,
Department of Molecular Pharmacology and Physiology, University of South Florida, 560 Channelside Dr., Tampa, FL 33602.
Contact number: 913-206-0264.
Email: rtiwari@usf.edu.

Alexander Staruschenko,
Department of Molecular Pharmacology and Physiology, University of South Florida, 560 Channelside Dr., Tampa, FL 33602.
Contact number: 813-396-0147.
Email: staruschenko@usf.edu.

SUPPLEMENTAL METHODS

Transcriptomic analysis

Analyses were conducted in RStudio (v4.3.1) using DESeq2, tidyverse, ComplexHeatmap, msigdb, enrichR, STRINGdb, and other required packages. Counts were processed using the variance-stabilizing transformation (VST) in DESeq2 for unsupervised dimensionality reduction and visualization. Principal component analysis (PCA) was applied using the prcomp function, and the first two components were plotted to assess organ- and time point-specific separation. Sample-sample Pearson correlations were computed on the full VST matrix and visualized as annotated heatmaps using pheatmap. To capture non-linear structure, uniform manifold approximation and projection (UMAP) embeddings were generated (uwot, n_neighbors = 15, min_dist = 0.1) and visualized with ggplot2. Volcano plots were generated using counts per gene ID per organ-time point combination, with upregulated, downregulated, and nonsignificant genes distinguished by color. For each comparison, DEGs were intersected across tissues and time points to identify shared and unique responses. Common DEGs were visualized using Venn diagrams based on gene symbols (VennDiagram), clustered heatmaps (pheatmap), and subjected to Gene Ontology Biological Process (GO-BP), Kyoto Encyclopedia of Genes and Genomes (KEGG), and Hallmark enrichment via clusterProfiler and msigdb. Enrichment was performed using an over-representation analysis (ORA) framework.

Pathway activity scoring and trajectory analysis

Transcriptome-wide pathway activity was quantified using 50 Hallmark gene sets (MSigDB v7.5.1). Pathway scores were computed as the mean \log_2 fold change (\log_2 FC) for all genes in each set across organ-time point combinations, yielding a 50×16 matrix. These scores were visualized as heatmaps, ridge plots (ggribbles), and Euclidean distance trajectories relative to baseline to capture global shifts. Inter-organ pathway similarity was evaluated using pairwise Pearson correlation of pathway vectors and displayed as correlation heatmaps. Hierarchical clustering (Ward's method, Euclidean distance) identified stable modules of co-regulated pathways, with cluster identity and biological function annotated. UMAP and multidimensional scaling (MDS) were applied to visualize higher-order pathway dynamics. Organ-specific patterns were highlighted by extracting the top 10 most variable pathways per tissue and plotting temporal trajectories. Directionality of pathway regulation (up vs. down) was summarized using stacked bar plots across time.

Protein-protein interaction analysis

To interrogate gene-level convergence, protein-protein interaction (PPI) networks were constructed for common DEGs at early (D7) and late (D35) time points using the STRING database (1) (v11, score > 700). Networks were clustered using Louvain community detection (2) (igraph) and annotated via module-level enrichment against Hallmark gene sets. Visualizations were rendered with ggraph, where nodes represent proteins sized by connectivity and colored by module identity.

Upstream transcription factor and network analysis

Transcription factor (TF) enrichment was performed using ChEA 2022 (3) via the enrichr R interface. To enable compatibility with human TF databases, rat DEGs were mapped to human orthologs using a tiered approach combining Ensembl BioMart, g:Profiler, and HomoloGene. Enrichment analysis was conducted separately for each organ and time point. The top 10 enriched TFs per condition were visualized using faceted bubble plots. A presence–absence matrix was used to classify TFs as shared or organ-unique and visualized using concentric donut plots and Venn diagrams. TF–target interactions were mapped using ChEA and overlaid with expression heatmaps to highlight regulatory architecture. Target gene sets were further subjected to GO and Hallmark pathway analysis.

To capture global variation in TF activity, dimensionality reduction was performed on the TF \log_2 FC matrix using PCA and UMAP. Organ-specific trajectories were visualized across the time course (D7 to D35). To determine the most organ-discriminative TFs at each time point, we trained Random Forest classifiers independently for each day using TFs \log_2 FC values as predictors and organ identity as the response variable. The mean decrease in Gini was used to rank TF importance and highlight top organ-informative regulators.

Transcriptomic-GWAS integration analysis

To link transcriptomic signatures with human disease relevance, we integrated rat DEGs with human GWAS loci for hypertension and CKD (NHGRI-EBI GWAS Catalog, release e114_r2025-05-13). Rat–human orthologs were derived as described above. Overlap statistics were evaluated using Fisher’s exact test and overlap genes (hypertension: $n = 100$; CKD: $n = 143$) were profiled across all organs–time point combinations. Z-score normalized heatmaps were used to assess expression dynamics. ORA (GO-BP, KEGG, Reactome) was performed using clusterProfiler and ReactomePA. PPI networks were reconstructed for overlap genes and analyzed using STRING and Louvain clustering to identify disease-relevant modules, which were annotated by GO enrichment and visualized with ggraph.

Drug perturbation analysis

To systematically identify compounds that can rescue salt-induced hypertension-associated transcriptional changes, ORA was performed against the Library of Integrated Network-Based Cellular Signatures (LINCS) L1000 chemical perturbation databases using enrichr (4). The LINCS L1000 resource provides a large compendium of gene-expression profiles elicited by hundreds of small molecules across diverse human cell types, thereby enabling direct linkage of disease signatures to candidate pharmacological modulators (5, 6). For each DEG set, upregulated genes were queried against LINCS_L1000_Chem_Pert_down signatures, representing compounds predicted to reverse the observed gene induction, whereas downregulated genes were tested against LINCS_L1000_Chem_Pert_up signatures, representing compounds predicted to restore suppressed gene expression. The top ten enriched compounds per group were retained. The enrichment results were merged and duplicate entries with identical compound labels collapsed by retaining the instance with the lowest adjusted P value. The compound terms that differed in

exposure time were also preserved as distinct entries. To provide complementary biological context for the chemical perturbation results, enrichment against the MSigDB Hallmark 2020 gene sets was conducted in parallel. For each gene set, the top five Hallmark pathways were selected based on adjusted P values, supporting the mechanistic interpretation of compound–disease relationships by anchoring transcriptional signatures within biological processes. Sankey diagrams were constructed to visualize temporal and pharmacological relationships. Edges connecting each time-point to enriched Hallmark pathways had line widths scaled as $5 \times (-\log_{10} \text{ adjusted } P \text{ value})$ to emphasize temporal signal strength, while edges linking pathways to LINCS compounds were weighted proportionally to the unscaled $-\log_{10}$ adjusted P value. Networks were generated using the networkD3 R package. Further, identified drugs were categorized manually based on their reported primary targets or mechanisms of action then collapsed into broader therapeutic categories: receptor tyrosine kinase (RTK) inhibitors (including compounds targeting EGFR, HER2, VEGFR, FGFR, ALK, and related kinases), MAPK pathway inhibitors (targeting BRAF, RAF, MEK, ERK, and p38), cell-cycle kinase inhibitors (encompassing CDK, PLK, and CHK inhibitors), PI3K/mTOR inhibitors, HSP90 inhibitors, and anti-inflammatory agents (including JAK, JNK, IKK, NF- κ B). Compounds that did not match any of these criteria were classified as “Other.” For each tissue and time point, we created an aggregate enrichment score by summing the $-\log_{10}$ of the adjusted P values for every compound in a given drug class. These class-level scores were winsorized at 5000 to prevent extremely small P values from dominating the visualization. Streamgraphs were then produced with the ggstream and ggplot2 R packages.

Histopathological analysis

For histological evaluation of the kidney, liver, and heart, tissue samples were fixed in 10% zinc-buffered formalin, and paraffin-embedded blocks were prepared. Sections of 4 μm thickness were cut and stained with Masson’s trichrome for fibrosis assessment and hematoxylin and eosin (H&E) for injury scoring. Whole-slide images were scanned, and quantitative analyses were performed using QuPath software (v0.5.1) (7). For kidney injury scoring, each whole-kidney section was divided into $1000 \times 500 \mu\text{m}$ fields, and the cortex and medulla were evaluated separately using a semi-quantitative scoring system. Scores were assigned based on the percentage of tissue area affected by necrosis, brush border loss, cast formation, and tubular dilation: 0 = no injury; 1 = <10%; 2 = 11–25%; 3 = 26–50%; and 4 = >50% injury in the field. More than 100 cortical fields and over 50 medullary fields per animal were analyzed. Fibrosis quantification was performed by calculating the percentage of Masson’s trichrome-positive area separately for cortex and medulla. In the heart and liver, perivascular fibrosis was quantified. Over 20 vessels per sample were selected based on size and shape. Collagen surrounding these vessels was measured as perivascular collagen. The percentage of collagen was calculated by analyzing the ratio of positively stained (blue) pixels to total pixels within each vessel's perivascular region. Histopathological assessment and analysis were conducted by investigators blinded to group allocation.

Serum and urine analysis

Electrolyte and creatinine concentrations in urine and plasma were measured using a blood gas analyzer (ABL800 FLEX, Radiometer America Inc.). Urinary albumin concentrations were quantified using a fluorescence-based dye-binding assay adapted for rat samples. A dilution series

of rat serum albumin standards (0.0032–0.2 mg/mL) was prepared in Buffer B (standard diluent: Milli-Q water with buffering salts), and rat urine samples were diluted 1:10 in the same buffer. Twenty-five microliters of each standard or sample were plated in duplicate into a 96-well plate. A working dye solution was prepared fresh by diluting lyophilized AM3 dye (resuspended in isopropanol) 1:50 in Buffer A, a MOPS-based buffer containing 10% isopropanol. Following the addition of 150 μ L of working dye per well, plates were incubated for 5 minutes at room temperature in the dark. Fluorescence was measured using a microplate reader (excitation: 560 nm; emission: 620 nm). Albumin concentrations were calculated by interpolating sample values from a standard curve, corrected for blank values, and dilution factor as reported previously (8).

REFERENCES

1. Szklarczyk D, et al. The STRING database in 2023: protein-protein association networks and functional enrichment analyses for any sequenced genome of interest. *Nucleic Acids Res.* 2023;51(D1):D638-D46.
2. Blondel VD, et al. Fast unfolding of communities in large networks. *J Stat Mech.* 2008;2008(10):P10008.
3. Lachmann A, et al. ChEA: transcription factor regulation inferred from integrating genome-wide ChIP-X experiments. *Bioinformatics.* 2010;26(19):2438-44.
4. Xie Z, et al. Gene Set Knowledge Discovery with Enrichr. *Curr Protoc.* 2021;1(3):e90.
5. Keenan AB, et al. The Library of Integrated Network-Based Cellular Signatures NIH Program: System-Level Cataloging of Human Cells Response to Perturbations. *Cell Syst.* 2018;6(1):13-24.
6. Subramanian A, et al. A Next Generation Connectivity Map: L1000 Platform and the First 1,000,000 Profiles. *Cell.* 2017;171(6):1437-52.e17.
7. Humphries MP, et al. QuPath: The global impact of an open source digital pathology system. *Comput Struct Biotechnol J.* 2021;19:852-9.
8. Rinschen MM, et al. Accelerated lysine metabolism conveys kidney protection in salt-sensitive hypertension. *Nat Commun.* 2022;13(1):4099.

SUPPLEMENTAL FIGURES

Figure S1. Effects of high salt diet on blood pressure and tissue-specific transcriptional profiles. **A.** Mean arterial pressure (MAP) in male Dahl SS rats fed normal salt (NS) or high salt (HS, 4% NaCl) diet. Two-way repeated-measures ANOVA was used. The inset box summarizes the two-way ANOVA results, showing significant main effects of time ($****P < 0.0001$) and diet ($**P < 0.01$), as well as a significant time and diet interaction ($****P < 0.0001$). Post hoc pairwise comparisons between HS and NS at each time point were performed with Šídák's correction and significance levels are indicated on the graph as $*P < 0.05$, $**P < 0.01$, $***P < 0.001$, and $****P < 0.0001$, with ns indicating not significant. Data are presented as mean \pm standard error of the mean (SEM). $n = 4$ – 9 male rats per group. **B.** Principal component analysis (PCA) of variance-stabilized (VST) RNA-seq counts from kidney cortex, kidney medulla, liver, and heart tissues obtained from a separate cohort (not subjected to telemetry surgery to avoid surgery-related transcriptomic changes) under NS conditions and after 7, 14, 21, and 35 days of HS diet. **C.** Rank-abundance distributions of log-transformed transcript counts for each organ across experimental time points. Genes are ordered from highest to lowest mean expression on the x-axis, with abundance plotted on the y-axis. Colored lines show consistent global transcript abundance distributions across organs and time points. CX, cortex; MD, medulla; LV, liver; HR, heart; D7, day 7; D14, day 14; D21, day 21; and D35, day 35 time points. $n = 6$ male rats per group.

Figure S2. Volcano plot analysis reveals organ-specific and temporal patterns of gene regulation under high salt diet-induced hypertension. Volcano plots showing differential gene expression (\log_2 fold change vs $-\log_{10}$ adjusted P value) in the kidney cortex, kidney medulla, liver, and heart at days 7, 14, 21, and 35 relative to their respective controls. Significantly upregulated genes are shown in red, downregulated genes in blue, and non-significant genes in gray. Numeric labels above each plot indicate counts of upregulated (Up), downregulated (Down), and non-significant (NS) genes. Genes with $|\log_2$ fold change| ≥ 0.585 , equivalent to a fold change ≥ 1.5 with adjusted $P < 0.05$ were considered significant. CX, cortex; MD, medulla; LV, liver; HR, heart; D7, day 7; D14, day 14; D21, day 21; and D35, day 35 time points. adj. p indicates adjusted P value. $n = 6$ male rats per group.

Figure S3. Electrolyte, histological, and molecular changes during salt-induced hypertension in Dahl SS rats. **A–E.** Electrolyte measurements showing urinary sodium-to-creatinine ratio (Na/Cr) (**A**), urinary chloride-to-creatinine ratio (Cl/Cr) (**B**), blood sodium (Na) (**C**), blood chloride (Cl) (**D**), and blood pH (**E**) in normal salt controls (NS) and at days 7, 14, 21, and 35 of high salt (HS) diet. **F.** Representative Masson's trichrome images of liver and heart from NS and HS diet-fed rats at days 7, 14, 21, and 35. Collagen (fibrosis) is blue; parenchyma/myocardium is red. Scale bars, 100 μm . **G.** Semi-quantitative analysis of Trichrome-positive area (%) in liver and heart (perivascular region) across time points. **H.** Heatmaps show \log_2 fold-change (vs NS) expression of selected genes associated with fibrosis and inflammation at each time point in liver and heart. Expression levels of genes were extracted from RNA-seq analysis. For **A–G**, Data are shown as mean \pm standard error of the mean (SEM). One-way ANOVA with Šídák's multiple comparisons test was used. Statistical comparison is vs NS; ns, not significant; $*P < 0.05$; $**P < 0.01$; $****P < 0.0001$; $n = 4$ – 8 male rats per group. For **H**, Asterisks denote Benjamini–Hochberg adjusted- P thresholds (adj. P). $*adj. P < 0.05$; $**adj. P < 0.01$; $***adj. P < 0.001$; $n = 6$ male rats per group. D7, day 7; D14, day 14; D21, day 21; and D35, day 35 time points. *Vcam1*, vascular

cell adhesion molecule 1; *Tgfb1*, transforming growth factor beta 1; *Icam1*, intercellular adhesion molecule 1; *Got1*, glutamic-oxaloacetic transaminase 1; *Col3a1*, collagen type III alpha 1 chain; *Loxl2*, lysyl oxidase like 2.

Figure S4. High salt diet-induced hypertension promotes progressive, region-specific injury in the kidney. Dahl SS rats were maintained on a normal salt (NS; 0.4% NaCl) or switched to a high salt (HS; 4% NaCl) diet for 7, 14, 21, or 35 days. **A.** Kidney weight normalized to body weight (g/kg). **B.** 24-hour urine volume (mL/day). **C.** Urine albumin-to-creatinine ratio (Alb/Cr). **D.** Serum creatinine concentration (mg/dL). **E.** Representative hematoxylin and eosin (H&E; top two rows) and Masson's trichrome (bottom two rows) staining of renal cortex and medulla from NS- and HS-fed rats at the indicated time points (scale bars show 100 μ m). **F–G.** Injury scores in cortex (**F**) and medulla (**G**). **H–I.** Percentage of cast-positive area in cortex (**H**) and medulla (**I**). **J–K.** Percentages of Masson's trichrome positive area in cortex (**J**) and medulla (**K**). Data are shown as mean \pm standard error of the mean (SEM); $n = 4$ –15 male rats per group. For **A–D** and **F–K**, one-way ANOVA with Šídák's multiple comparisons was used. * $P < 0.05$; ** $P < 0.01$; *** $P < 0.001$; **** $P < 0.0001$; ns, not significant. **L.** Heatmaps of selected genes associated with injury, fibrosis, and inflammation showing \log_2 fold-change (vs NS) at each time point in cortex and medulla. Expression of genes was extracted from RNA-seq analysis. On the heatmap, asterisks denote Benjamini–Hochberg adjusted P thresholds (*adj. P*). **adj. P* < 0.05; ***adj. P* < 0.01; ****adj. P* < 0.001; $n = 6$ male rats per group. D7, day 7; D14, day 14; D21, day 21; and D35, day 35 time points. *Haver1*, hepatitis A virus cellular receptor 1 (kidney injury molecule-1); *Lcn2*, lipocalin 2; *Spp1*, secreted phosphoprotein 1; *Loxl2*, lysyl oxidase like 2; *Acta2*, actin alpha 2, smooth muscle; *Tgfb1*, transforming growth factor beta 1; *Colla1*, collagen type I alpha 1 chain; *Colla2*, collagen type I alpha 2 chain.

Figure S5. Temporal dynamics of highly variable pathways across organs. Line plots showing temporal trajectories of the top 10 most variable Hallmark pathways within each tissue. The dotted line denotes control levels; pathways above the line are upregulated, while those below are downregulated. CX, cortex; MD, medulla; LV, liver; HR, heart; D7, day 7; D14, day 14; D21, day 21; and D35, day 35 time points. $n = 6$ male rats per group.

Figure S6. Unsupervised clustering of Hallmark pathway trajectories. **A.** UMAP visualization of Hallmark pathway profiles shows four distinct clusters based on their expression patterns across different tissues and time points (days 7–35). Each point represents a pathway, colored by its assigned cluster. Pathways in Cluster 1 (red) are enriched for mitochondrial and lipid metabolism processes. Cluster 2 (blue) includes immune and inflammatory response pathways. Cluster 3 (green) contains a broad range of metabolic, stress response, and developmental pathways. Cluster 4 (purple) groups cell cycle-related pathways including E2F targets and G2M checkpoint. **B.** Silhouette score plot used to determine the optimal number of clusters ($k = 4$), based on average silhouette width across $k = 2$ –8. EMT, epithelial–mesenchymal transition. $n = 6$ male rats per group.

Figure S7. GO Biological Process (GO-BP) enrichment of genes commonly dysregulated across all four tissues in high salt diet-induced hypertension. Differentially expressed genes shared among the kidney cortex, kidney medulla, liver, and heart at days 7 and 35 were analyzed

for Gene Ontology Biological Process (GO-BP) enrichment. **A** and **B** show results for day 7, with panel **A** depicting the top 10 enriched GO-BP terms and panel **B** showing the GO-BP enrichment map visualizing semantic similarity networks among enriched terms. **C** and **D** show results for day 35, with panel **C** depicting the top 10 enriched GO-BP terms and panel **D** showing the GO-BP enrichment map visualizing semantic similarity networks among enriched terms. Node size reflects gene set size and color intensity indicates statistical significance. D7, day 7; D35, day 35; adj. p, adjusted P value. $n = 6$ male rats per group.

Figure S8. High salt diet-induced hypertension dynamically regulates biological processes across organs and time points. Bubble plots show the top 5 enriched GO Biological Process (GO-BP) terms (adjusted $P < 0.05$) identified from all significant differentially expressed genes ($|\log_2$ fold change $|\geq 0.585$, equivalent to a fold change ≥ 1.5 with adjusted $P < 0.05$) in the kidney cortex, kidney medulla, liver, and heart at days 7, 14, 21, and 35. Dot size represents the number of overlapping genes, and color denotes statistical significance ($-\log_{10}$ adjusted P). Results highlight dynamic organ- and time-specific regulation of processes including cell division, immune response, metabolic activity, and tissue-specific programs. CX, cortex; MD, medulla; LV, liver; HR, heart; D7, day 7; D14, day 14; D21, day 21; and D35, day 35 time points. adj. p indicates adjusted P value. $n = 6$ male rats per group.

Figure S9. Distinct temporal and organ-specific Hallmark pathways engaged by high salt diet-induced hypertension. Bubble plots depict the top enriched Hallmark pathways (adjusted $P < 0.05$) derived from significantly altered genes ($|\log_2$ fold change $|\geq 0.585$, equivalent to a fold change ≥ 1.5 with adjusted $P < 0.05$) in the kidney cortex, kidney medulla, liver, and heart at days 7, 14, 21, and 35. Circle size indicates the number of overlapping genes, and color denotes statistical significance ($-\log_{10}$ adjusted P). CX, cortex; MD, medulla; LV, liver; HR, heart; D7, day 7; D14, day 14; D21, day 21; and D35, day 35 time points. adj. p indicates adjusted P value. $n = 6$ male rats per group.

Figure S10. Transcription factor enrichment analysis using ChIP-X Enrichment Analysis (ChEA) reveals dynamic, tissue- and time-specific regulators of high salt diet-induced hypertension. Bubble plots show the top enriched transcription factors identified by ChEA analysis (adjusted $P < 0.05$) using significantly altered genes from the kidney cortex, kidney medulla, liver, and heart at days 7, 14, 21, and 35. Dot size represents the number of overlapping target genes regulated by each transcription factor, while color intensity denotes statistical significance ($-\log_{10}$ adjusted P). Results highlight distinct temporal and tissue-specific TFs underlying hypertension-associated transcriptional remodeling. TF, transcription factors; CX, cortex; MD, medulla; LV, liver; HR, heart; D7, day 7; D14, day 14; D21, day 21; and D35, day 35 time points. adj. p indicates adjusted P value. $n = 6$ male rats per group.

Figure S11. Temporal dynamics and organ-specific divergence of transcription factor programs in response to high salt diet-induced hypertension. **A.** Heatmap showing \log_2 -fold changes of 79 transcription factors differentially expressed ($|\log_2$ fold change $|\geq 0.585$, equivalent to a fold change ≥ 1.5 ; adjusted $P < 0.05$) across the kidney cortex, kidney medulla, liver, and heart. **B.** Principal Component Analysis (PCA, top) and Uniform Manifold Approximation and Projection (UMAP, bottom) of transcription factor \log_2 -fold-change profiles, capturing tissue and

temporal trajectories from day 7 to day 35. Time points were connected sequentially to guide visualization of transcriptional shifts across the disease course within each tissue. Divergent transcription factor program evolution is most evident in the medulla and liver, with subtler differences in the heart and cortex. **C.** Top ten transcription factors most discriminatory for organ type at each time point, identified by Random Forest classification. Bar lengths indicate variable importance, measured by mean decrease in Gini, reflecting dynamic shifts in transcriptional regulators that drive organ-specific responses over time. TF, transcription factors; CX, cortex; MD, medulla; LV, liver; HR, heart; D7, day 7; D14, day 14; D21, day 21; and D35, day 35 time points. $n = 6$ male rats per group.

Figure S12. Integration of Dahl SS rat transcriptome with human genome-wide association studies (GWAS) loci identifies conserved gene networks underlying hypertension and kidney disease. **A and B.** Integration of rat transcriptomic data with human GWAS identified a significant enrichment of overlap genes associated with hypertension (**A**) and chronic kidney disease (CKD; **B**). Venn diagrams show the intersection between rat DEGs and GWAS loci-associated genes, revealing non-random convergence (hypertension: $P < 0.0001$, odds ratio = 2.4; CKD: $P < 0.0001$, odds ratio = 3.8; Fisher's exact test). **C and D.** Enriched pathways from GWAS-overlapping genes revealed coherent biological processes in hypertension (**C**), and CKD-overlap genes (**D**). **E and F.** Protein-protein interaction (PPI) networks constructed from GWAS-overlap genes, revealing distinct modular architectures (STRING: score > 400 for hypertension, > 700 for CKD). Louvain clustering identified discrete protein communities, each annotated by its most significantly enriched GO-BP term. Node size corresponds to degree centrality; edge width reflects interaction strength; colors denote module identity. adj. p indicates adjusted P value.

Figure S13. Temporal and organ-specific dynamics of genes overlapping human GWAS loci for hypertension and chronic kidney disease in salt-induced hypertension. **A and B.** Heatmaps showing Z-scored \log_2 fold-changes of rat orthologs overlapping with human GWAS loci for hypertension (**A**) and chronic kidney disease (CKD; **B**) across the kidney cortex, kidney medulla, liver, and heart at days 7, 14, 21, and 35 following high salt diet in Dahl SS rats. CX, cortex; MD, medulla; LV, liver; HR, heart; D7, day 7; D14, day 14; D21, day 21; and D35, day 35 time points. $n = 6$ male rats per group.

Figure S14. GWAS-overlap genes reveal divergent biological pathways for hypertension and chronic kidney disease in Dahl SS rats. **A.** Comparative Gene Ontology Biological Process (GO-BP) enrichment reveals disease-specific biological processes enriched in the hypertension and CKD overlap sets. **B and C.** KEGG and Reactome enriched terms for hypertension-overlap genes. Top pathways include cortisol and renin synthesis and secretion, ECM-receptor interaction, and extracellular matrix organization, implicating stress-responsive and structural remodeling pathways in hypertensive injury. **D and E.** KEGG and Reactome enriched terms of CKD-overlap genes reveal enrichment of metabolic processes, including fatty acid oxidation, cytochrome P450-mediated detoxification, bile acid transport, and tryptophan metabolism. adj. p indicates adjusted P value.

Figure S15. Temporal and organ-specific prediction of small molecules targeting downregulated gene programs in salt-induced hypertension. **A–D.** Sankey diagrams

integrating differential expression profiles with LINCS L1000 chemical perturbation signatures for significantly downregulated genes in the kidney cortex (**A**), kidney medulla (**B**), liver (**C**), and heart (**D**). Each network connects time points (D7–D35; left), enriched top five Hallmark pathways (middle), and the top predicted small molecules (right) prioritized for their potential to restore suppressed biological programs. Edge thickness denotes $-\log_{10}$ (adjusted P value), indicating enrichment strength. CX, cortex; MD, medulla; LV, liver; HR, heart; D7, day 7; D14, day 14; D21, day 21; and D35, day 35 time points. $n = 6$ male rats per group.

Figure S1

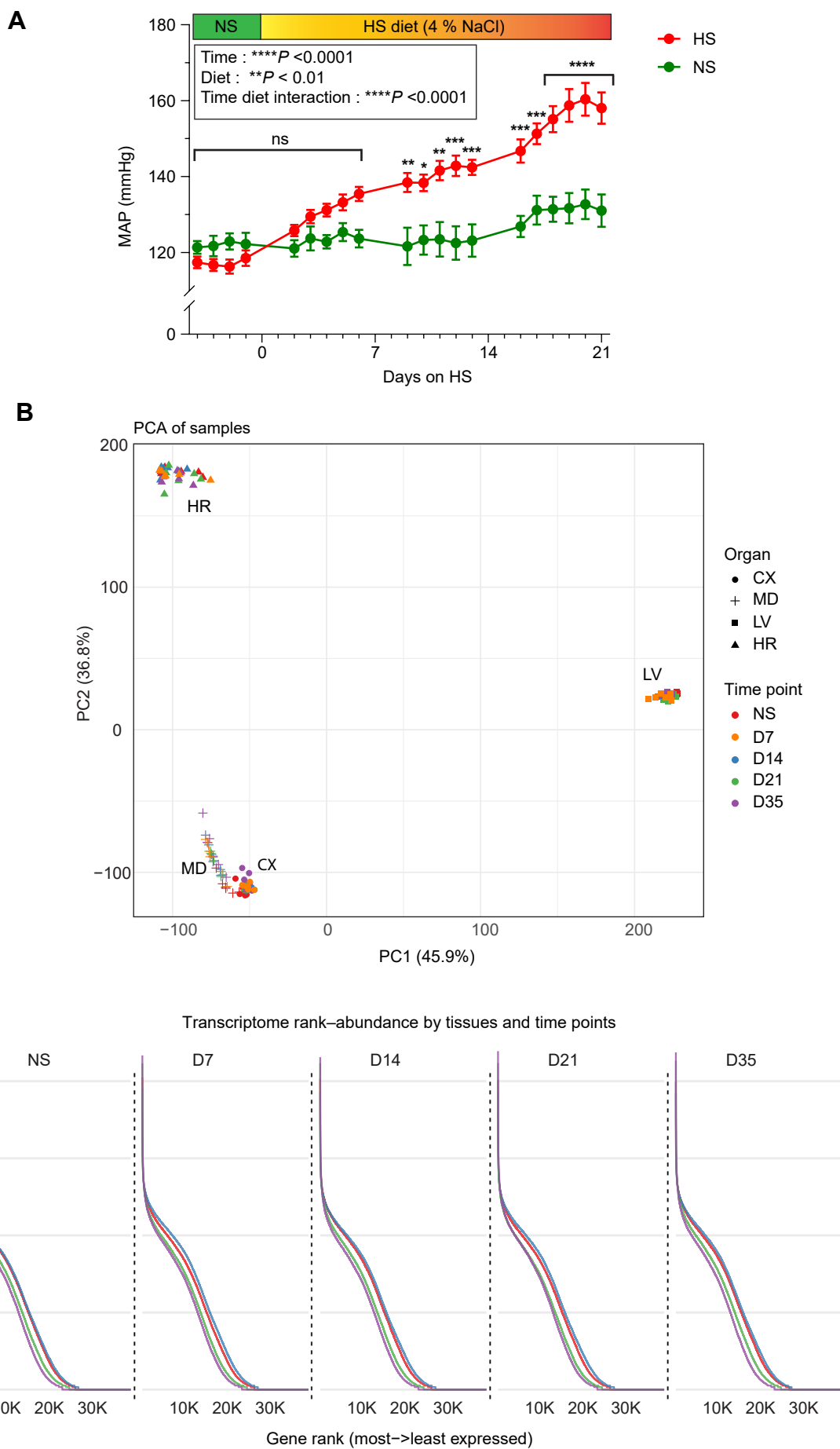
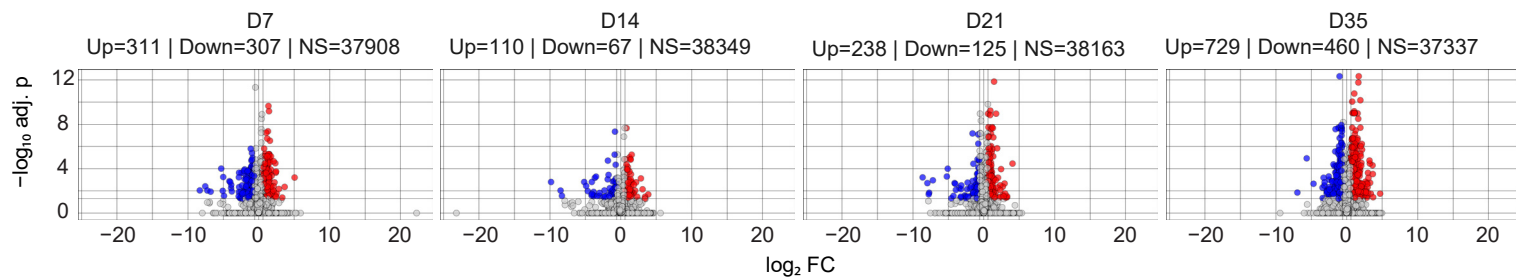
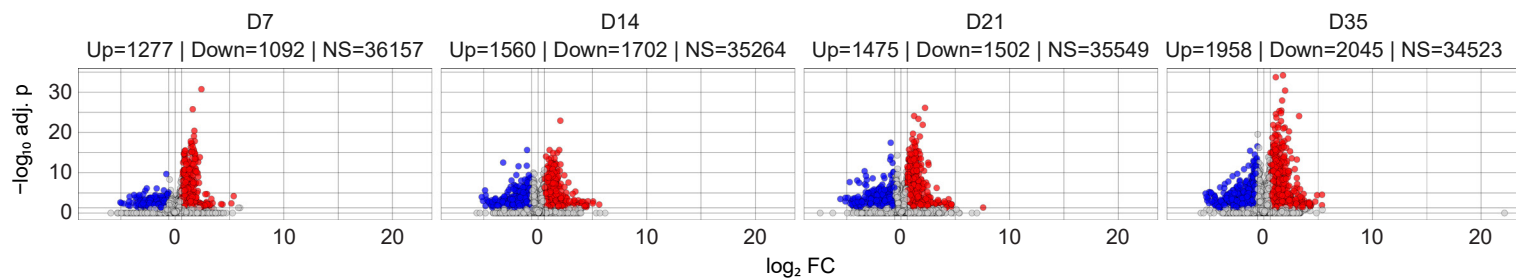


Figure S2

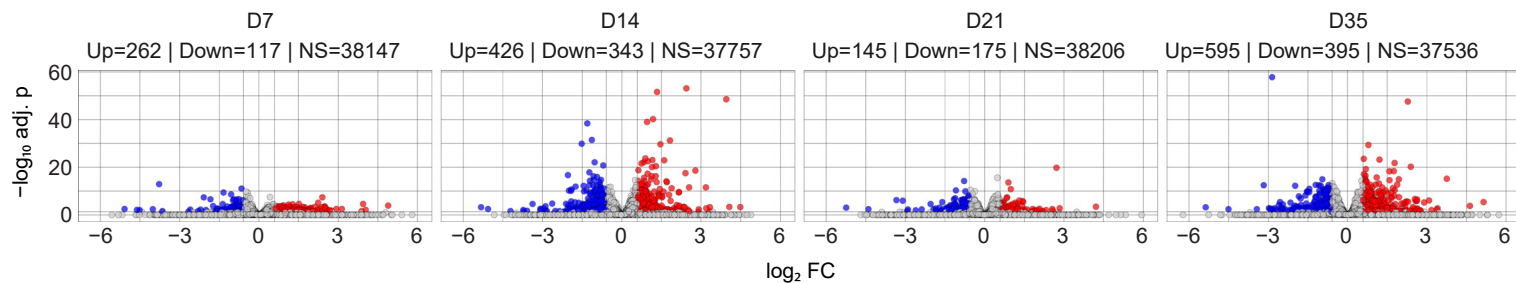
Volcano plot – CX



Volcano plot – MD



Volcano plot – LV



Volcano plot – HR

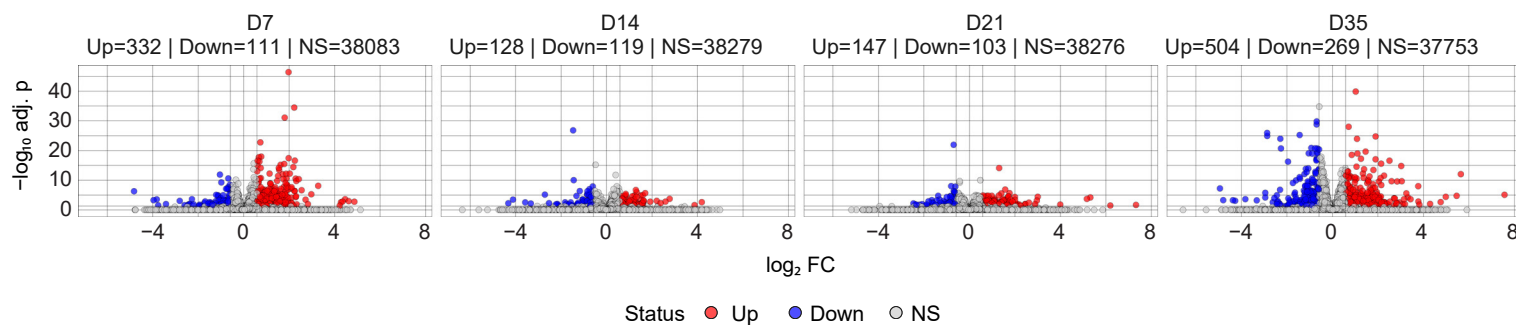


Figure S3

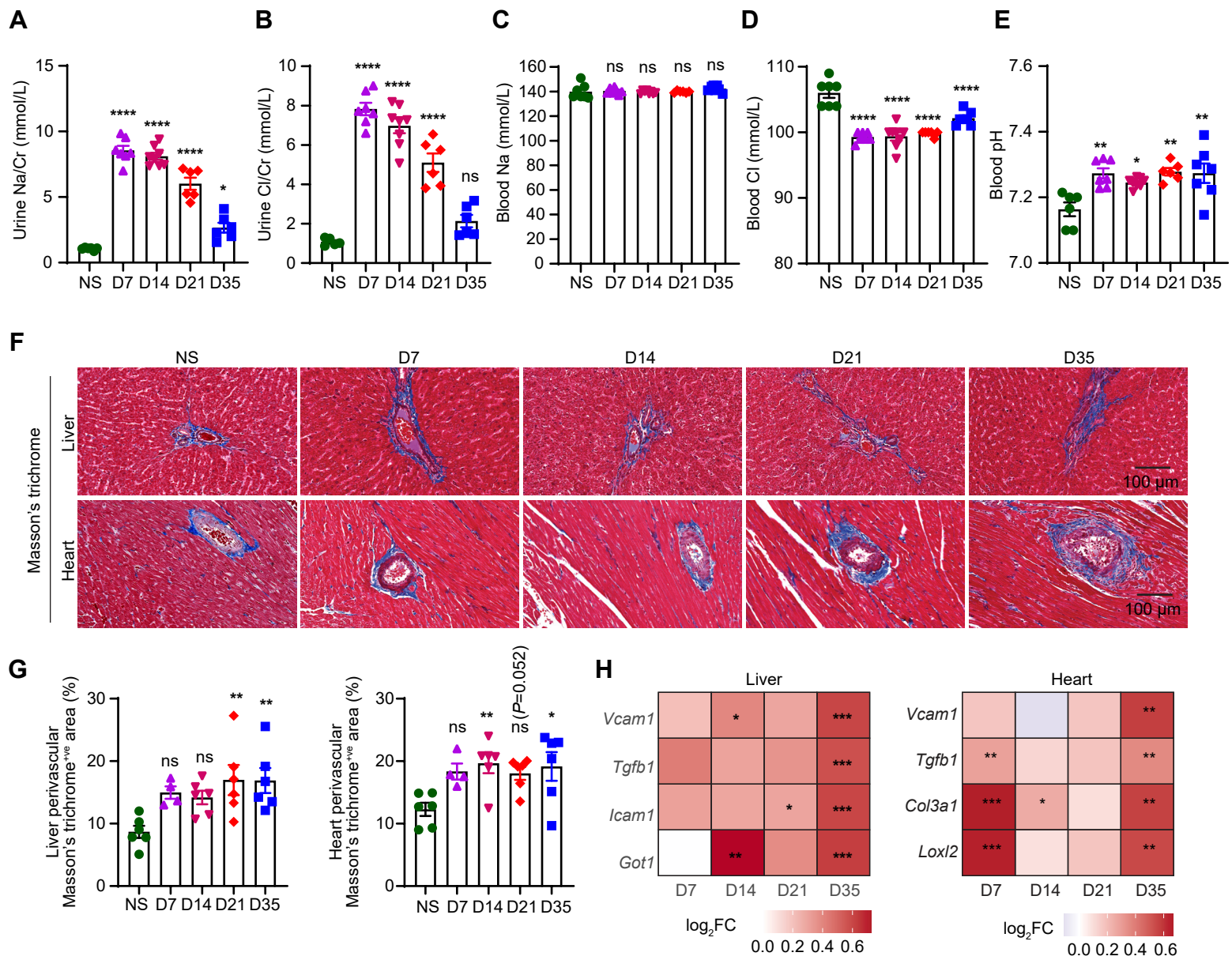


Figure S4

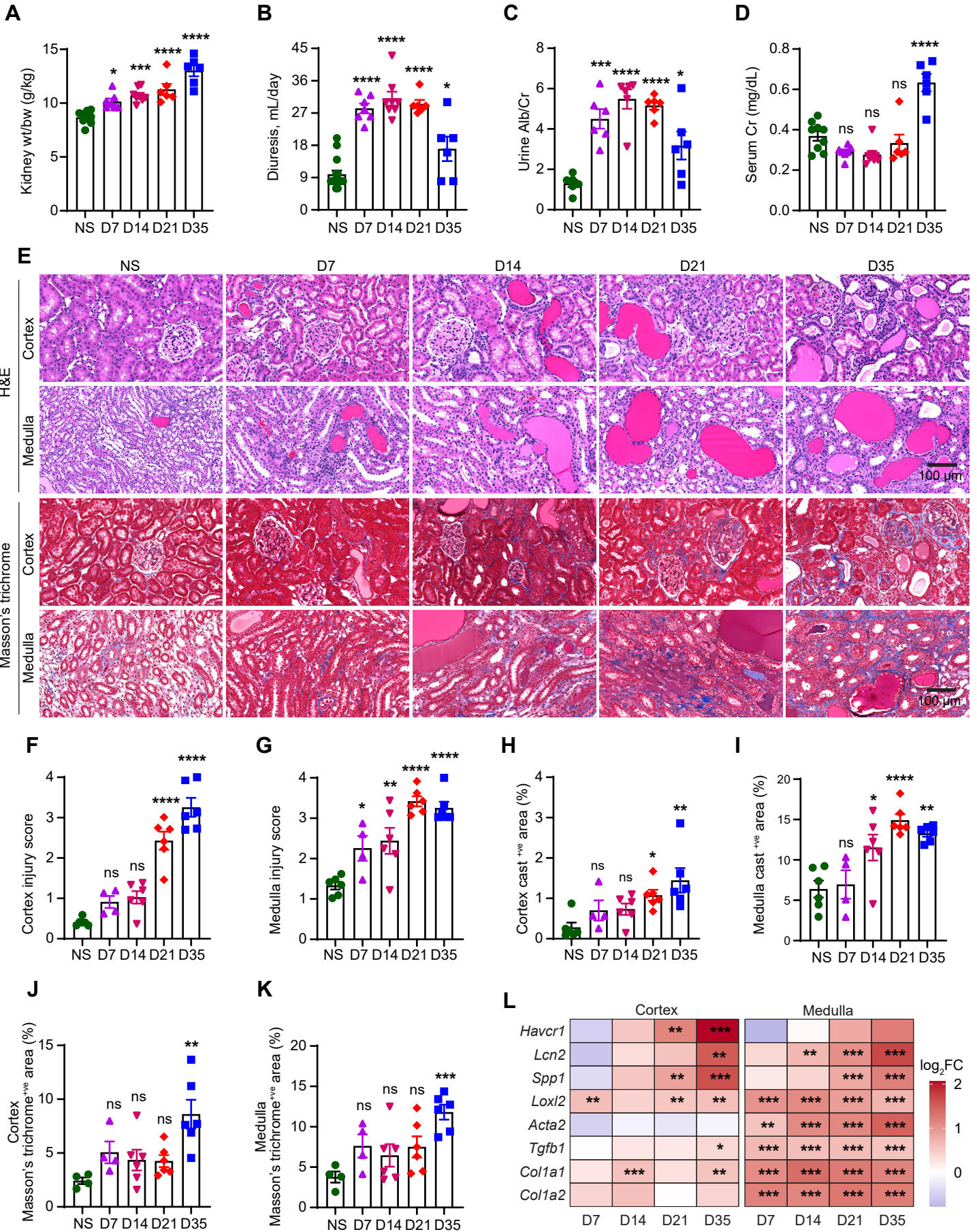
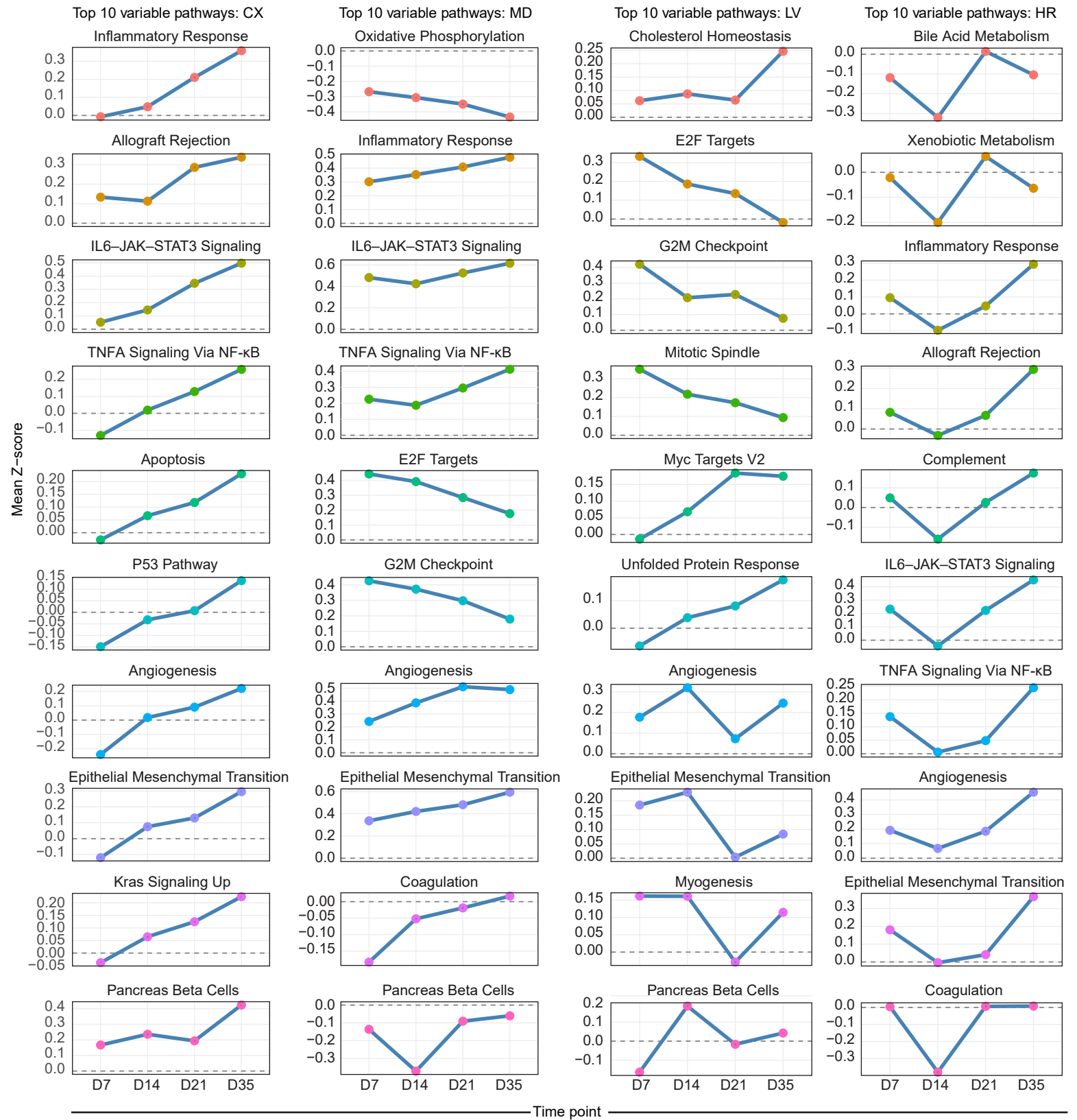


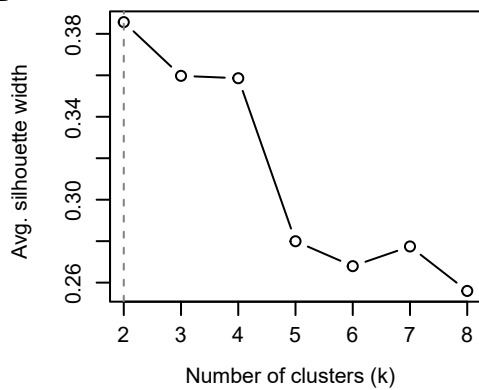
Figure S5



A UMAP of pathway profiles across tissues and time points



B Silhouette scan



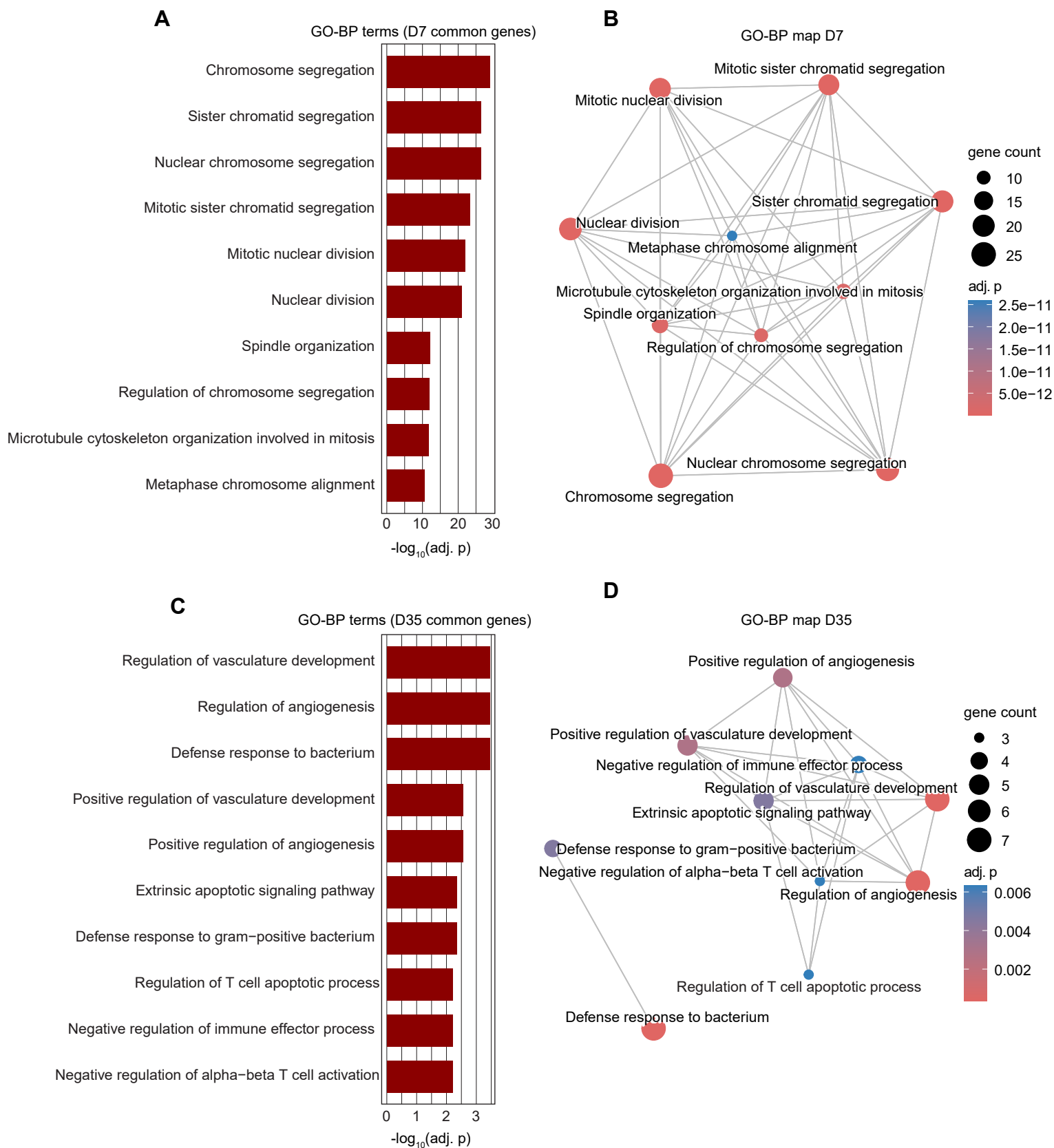


Figure S8

Top 5 GO-BP terms with adj. p < 0.05 from all significant DEGs

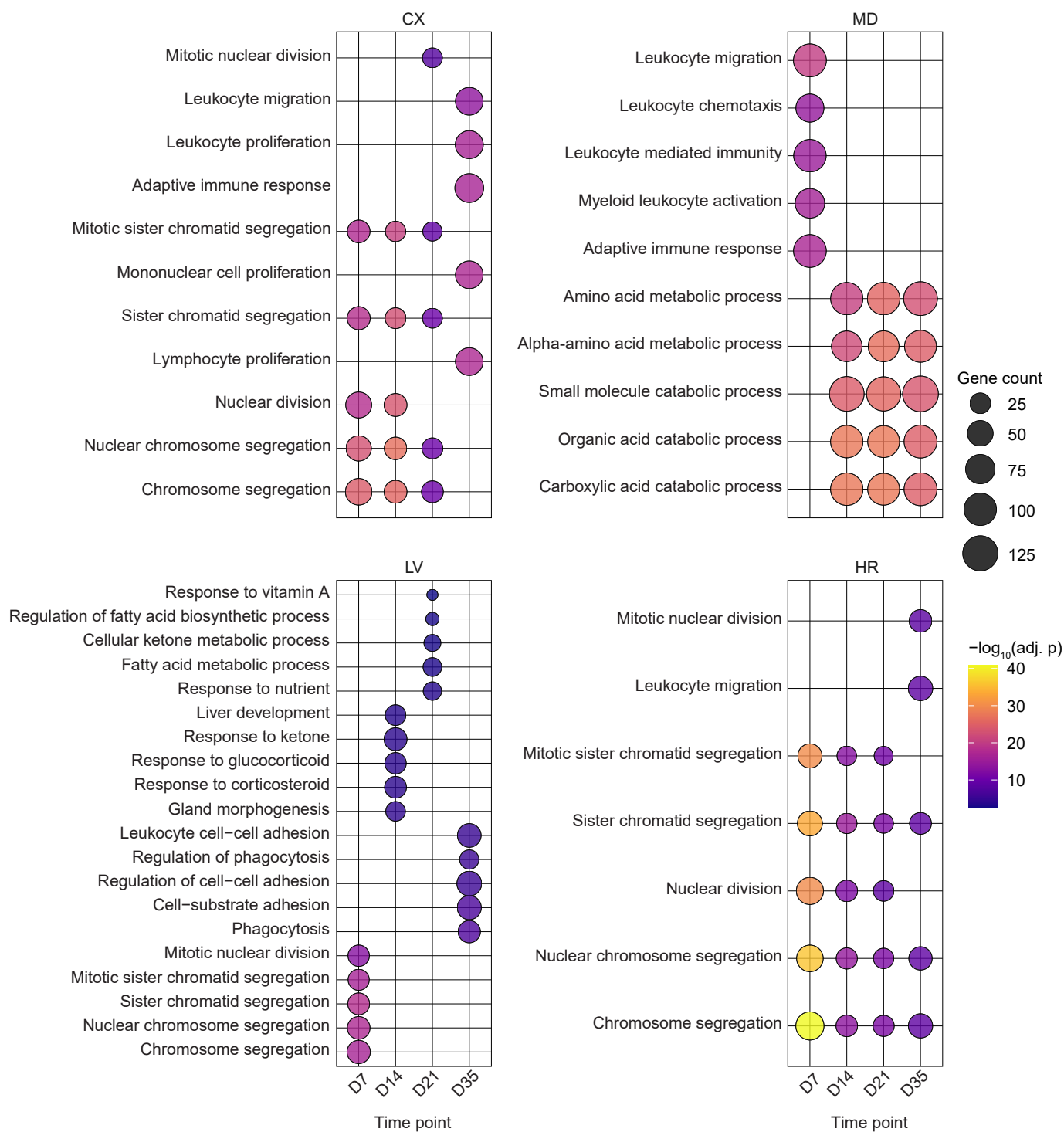


Figure S9

Top 5 Hallmark terms with adj. p < 0.05 from all significant DEGs

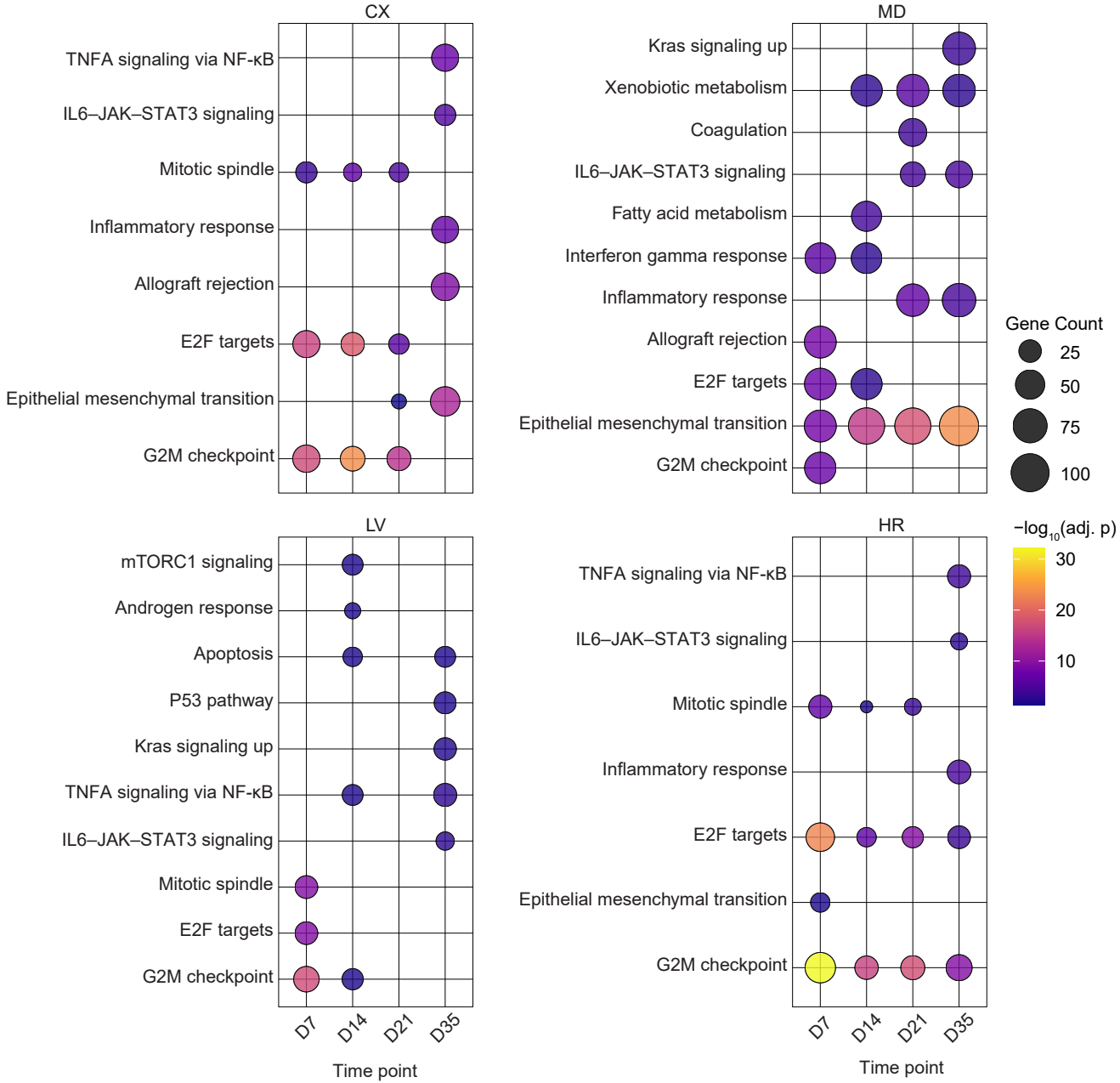
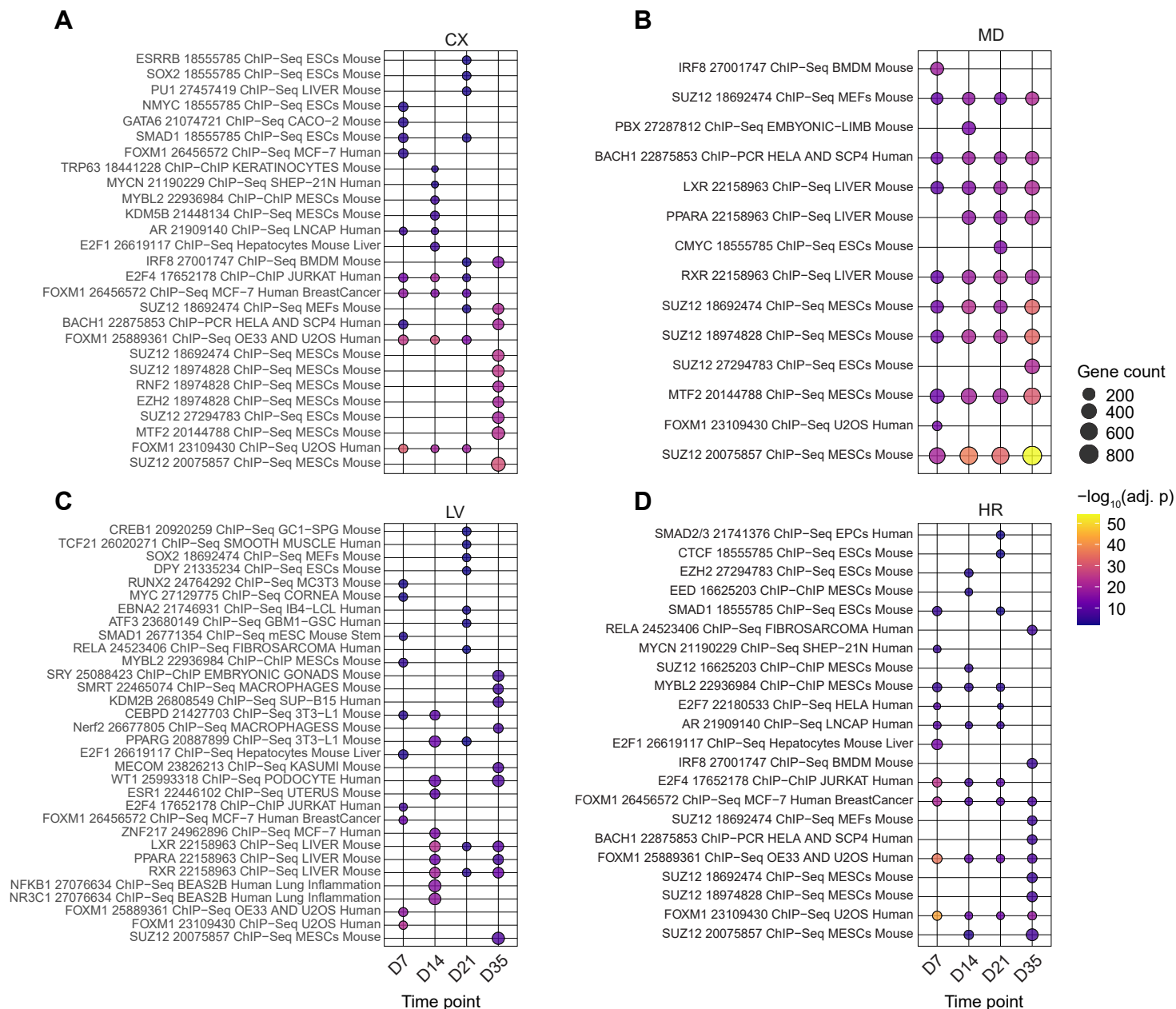
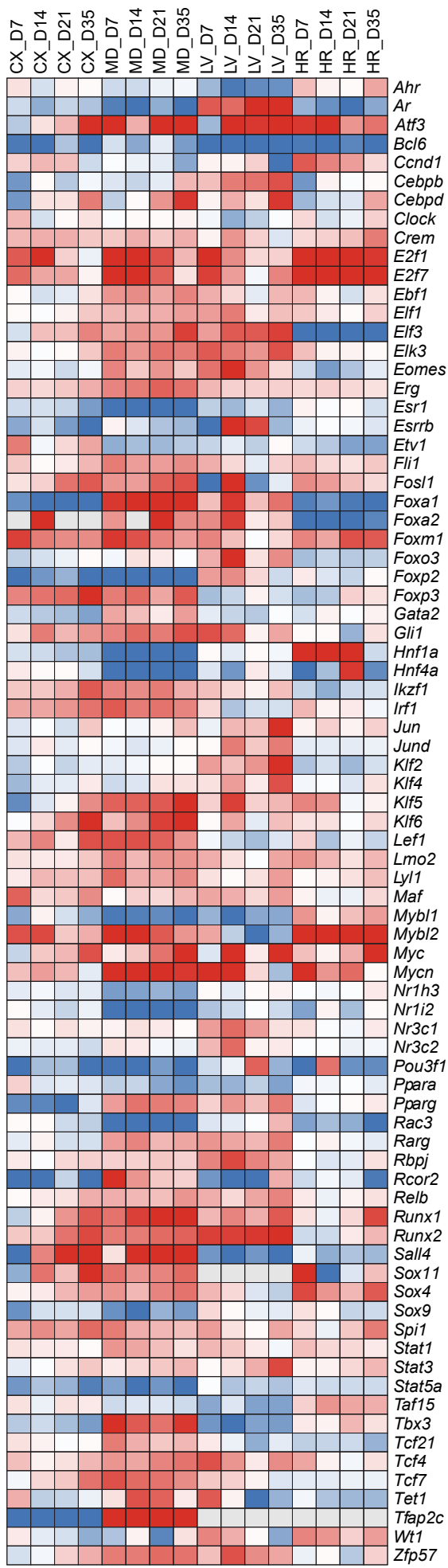


Figure S10

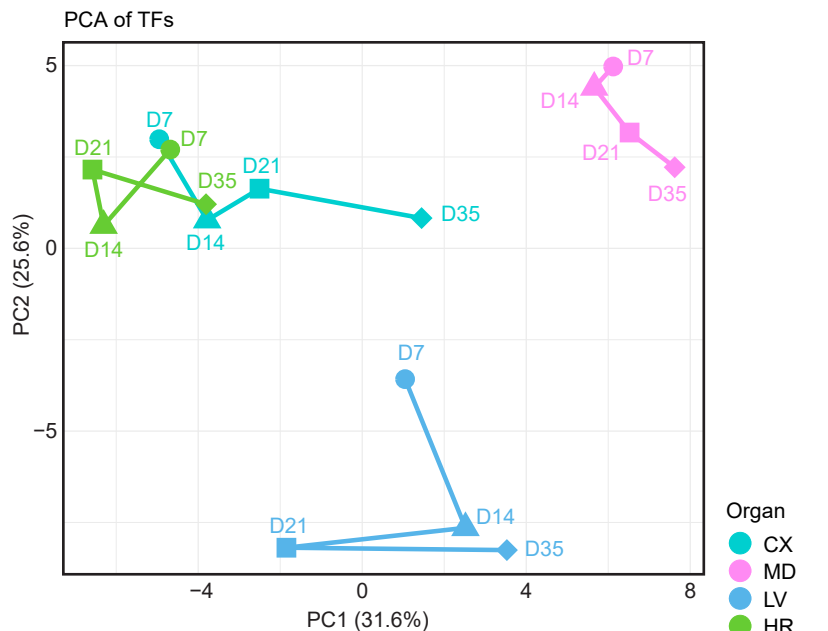
Top 10 ChEA 2022 TF terms across tissues and time points



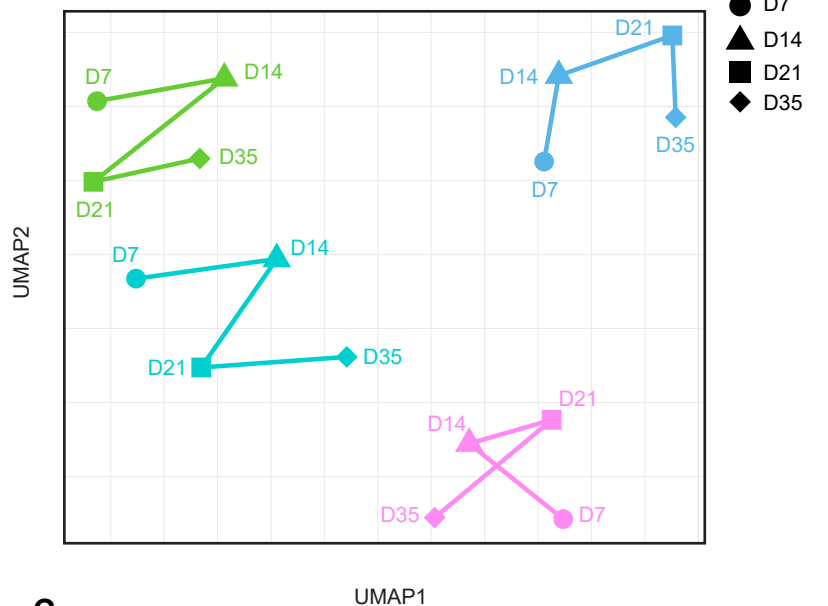
A



B



UMAP of TFs



C

